Developments on auxetic closed cell foam pressure vessel fabrications

O. Duncan[1], G. Leslie[1], S. Moyle[1], D. Sawtell[1] and T. Allen[1]
[1] Manchester Metropolitan University, Manchester, M15 6BH, UK

Key Words

Negative Poisson's ratio; Digital Image Correlation; Protective Equipment; Metamaterial; Manufacture

Abstract

Auxetic foam can have higher indentation resistance, better protection under impact and higher vibration damping than conventional foam. Unlike auxetic open cell foam, with established, commercially viable options for manufacturing, methods for making auxetic closed cell foam are not established. We revisited pressure-vessel methods, proposed in 1996, for making auxetic closed cell foam. We processed low-density polyethylene foam for six hours at 400 to 700 kPa and 100 °C, causing foams to shrink by a factor of two to five. The volumetric compression kinked cell walls, producing negative Poisson's ratios as low as -0.2 and Young's moduli from 0.2 to 1.2 MPa. Trends between applied volumetric compression and Poisson's ratio agree with those for open cell foam – initially decreasing to negative values as volume reduced by a factor of two after processing, then plateauing or slightly increasing as volume decreased by a factor of two to five. Foams of different sizes and shapes (15 to 75 mm sides) processed in the same conditions (700 kPa, 6 hours, 100 °C) shrank evenly in all three axes and had similar final volume ratios. We noticed a long settling period, of up to three months, where foams slowly shrank. Placing foam in a vacuum after processing reduced the settling period to within 24 hours.

1. Introduction

Auxetic foam [1] has a negative Poisson's ratio, meaning it expands in one or more transverse axis during tension, or contracts transversely during compression. Auxetic foam, and auxetic lattice metamaterials with macro- [2–4], micro- [5] and nano-scale [6] unit cells could improve sporting (and other) protective equipment, footwear [7–10], and composite sandwich structures [11–14]. Potential benefits of auxetic behaviour include unique shape change (e.g., domed curvature), which could improve equipment fit and comfort [5,15], high indentation resistance [7–9] and vibration damping [11,12], and high energy absorption before exceeding a threshold force associated with increased injury risk [8,10,16]. Indeed, auxetic materials are a class of smart material [17] – reacting to shape (e.g. of impacting bodies [8]), deformation type [18,19], and the speed of travelling waves within the material [14]. Sporting protective equipment, footwear and prosthetics often use closed cell foam as padding, with Young's moduli of about 1 MPa or more [20,21]. Closed cell foam can also prevent absorption of water or other contaminants, and heat loss by convection. Such stiff, insulating, water/contaminant resistant foam is also used in applications like bone surrogates [22], medical devices [23], protective equipment for defence [24], and in aerospace [25] and marine vessels [26].

Auxetic open cell foam was first made in the 1980s [27], by compressing conventional open cell foam to buckle cell walls, then heating and cooling to fix the imposed re-entrant structure.

Commercially viable methods have been proposed for making auxetic open cell foam (e.g. [9,28–31]), with associated patents (e.g. [31–34]). Auxetic (and conventional) open cell foam is typically softer than closed cell foam [8], undergoes stark changes in mass, volume, and other mechanical properties when wet [35,36], absorbs other contaminants [36], and allows convection [37].

Methods for making auxetic closed cell foam [38–42] are less established than those for auxetic open cell foam. As open and closed cell foam are not interchangeable, development of auxetic closed cell foam fabrication methods is needed. Recent work has used a steaming process to make auxetic closed cell foam [40,41]. Steam processing works by allowing steam to be absorbed into closed cells, causing them to shrink and form kinked cell walls as it condenses, giving a re-entrant cellular structure and auxetic behaviour. The foam polymer can be fixed over time if it passes through a transition temperature as the steam condenses [40,41]. Steaming uses simple equipment (container and conventional oven), but may be unsuitable for mass production, as it is slow, and processing conditions vary with sample shape and size [40]. While water evaporates from sheets of closed cell foam after steaming [43], increasing sample size (particularly thickness) may cause it to be trapped for longer. Steam processing also excludes polymer foams that melt or degrade notably below 100 °C – like polyurethane [1,44] and Ethylene-Vinyl-Acetate (EVA) [45–47], which are common in sports products like running shoes. Rapid "one-pot" steaming and foaming methods, in autoclaves with adjustable pressure settings, have also made auxetic closed cell foams [38,39]. These steam based "one-pot" methods have similar limitations (so far) to the steaming process described above [40,41]. The next challenge is to develop auxetic closed cell foam fabrication methods for larger samples, with fine control over cellular structure, which can be applied to various polymers.

Building on early, unrepeated work published in 1996 [42], we used a pressure vessel and oven to make auxetic closed cell foam. The method combines heat and pressure to soften and compress the foam, followed by cooling with the pressure retained to fix the re-entrant cellular structure. We clarified methods, investigated whether faster fabrication was possible and whether processing conditions (time, temperature & pressure) were sensitive to sample size.

2. Methods

2.1 Fabrication

Pressure vessels (140 mm long, internal diameter 50 mm) were made by adapting vacuum fittings (Edwards Vacuum – NW50 Full Nipple Stainless Steel and fittings – see supplementary assembly details (Figure S1), bill of materials (Table S1), and operational procedures). The vessels were used inside ovens, with the instrumentation (pressure gauge, thermo-couple reader and valve/pump) outside the ovens. Environmental conditions (temperature and relative humidity) were recorded during every measurement, test and processing cycle.

Processing time and temperature were first explored. Thirty-five closed cell foam samples of various sizes (15 to 75 mm sides) and densities (PlastaZote LD-24 and LD-45, **Figure 1**) were

processed. These foams were similar to those used for steam processing [40,48]. These were both closed cell low-density polyethylene foams, with stated densities of 24 and 45 kg/m^3. Similar stiffness (~1 MPa) polyethylene foam (including PlastaZote LD-45) is used in footwear [49–51], prosthesis [52] and sporting protective equipment [20,21]. Foam samples were placed in unpressurised vessels, within ovens, and then pressurised to between 400 and 700 kPa (gauge pressure). Ovens were set to 100 °C, close to the measured foam melting temperature of 108 °C (see Figure S2), and the pressurised vessels housing the foams were left for six hours. The air temperature inside the vessels reached 99 ± 0.5 °C (mean ± standard deviation) after half an hour. After six hours, the oven was switched off, and the vessel and foam were left to cool for an hour (with internal air temperature reaching 23 ± 2°C – Figure S3), before depressurising using the external valve. Pressure was checked and adjusted (if needed) every two minutes during heating and cooling to prevent safe working limits being exceeded, varying by up to 25 kPa above or below the set pressure. While health and safety requirements prevented longer overnight conversions, the effect of cumulative duration was assessed by processing for one, two or three six-hour cycles (six, 12 or 18 hours in total), typically on consecutive days.

Initially, one ~25 mm sided cube of LD-45 foam was processed for each condition (12 in total – 400 to 700 kPa, one to three cycles), along with three further LD-24 samples at 700 kPa (one for one cycle, and two for two cycles). For the initial tests on these cubes, 700 kPa and one cycle were found to consistently provide a final volume ratio (FVR = final/original volume) of about three to four – a target value based on previous work [40–42,48]. As such, a further seven ~25 mm sided cubes of each foam density (LD-24 & LD-45) were processed using these conditions of interest (700 kPa and one cycle), along with three smaller (15 × 25 × 25 mm) and three larger (75 × 25 × 25 mm) LD-45 samples. These samples of varying sizes were split between the three pressure vessels, with a small and a large one in each, to mitigate any effects of vessel conditions.

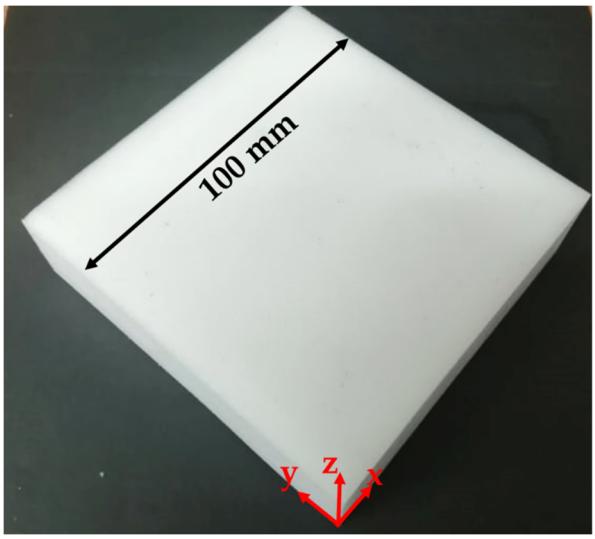

Figure 1: *An LD-45 unconverted foam cuboid (100 × 100 × 25 mm) that cubes were cut from using a utility knife's blade (Stanley), and axis labelling convention used throughout (z was through thickness). The LD-24 cuboid looked the same.*

Samples shrank for up to three months after conversion (Supplementary Figure S4), which could be problematic for commercial production. Based on the assumption that this long settling time was caused by air trapped within closed cells slowly dispersing over time (Figure 2), postprocessing (compression and suction, applied separately) was applied to foam cubes processed in the conditions of interest. Three cubes of each foam density were compressed to 80% engineering strain along their z-axis (Hounsfield HK10S uniaxial test device with a 5 kN load cell) at a strain rate of 0.0267 s^{-1}, then held for six hours, followed by the same amount and rate of compression in their x- and y-axis (without a holding period). Suction was applied to one cube of each type of foam, in a vacuum chamber (Teer Coatings, UDP450) pumped down to an absolute pressure of 1.1×10^{-5} Pa and left overnight (~17 hours).

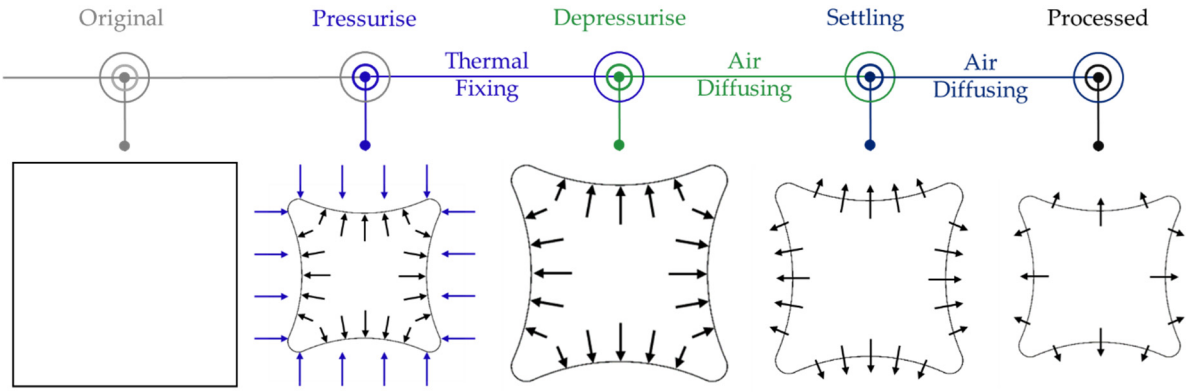

Figure 2: *Schematic showing foam volume change over time – with black and blue arrows representing air inside and outside foam cells, respectively.*

2.2 Foam measurements

Foam size measurements (Vernier Calipers), in all three axes at the centre of opposing faces, and masses (Sartorius, AC210S), were taken before and after processing, and about every seven days thereafter.[1] FVR reduced gradually after processing – as expected [42]. Foams were considered to have settled when the standard deviation of the weekly FVR measurements was under 10% of the mean FVR measured over three previous weeks (i.e., <3.5% which was ~0.5 mm variation in each axis). Foams left in the vacuum chamber overnight were measured after removal; daily for five days, then weekly for a month.

2.3 Cellular Structure

Optical microscopy was applied to view foam cellular structures, using an S-100 stereo microscope with 3 × optical zoom, a backing light (only), drapes to remove room light, and high contrast settings on the camera. Samples were sliced at a thickness of ~1 mm from processed (FVR ~3, 4 and 5) and unconverted samples to better show the cellular structures.

2.4 Mechanical Testing

ASTM D3574–11 was followed where possible, although the small size of the vessels – and hence produced samples – did not allow tests of 50 × 50 × 25 mm compression samples, nor the stamping of "dog-bone" tensile samples [53]. Laboratory conditions during testing were

[1] Some unavoidable breaks resulted from local lockdowns, laboratory closures and staff isolation.

21.75 ± 1.13 °C with a relative humidity of 34.28 ± 2.35% (below the 50% stated in ASTM D3574–11).

Compression tests to 20% engineering strain were applied to all foam cubes, in three orthogonal axis – first z, then x, then the y-axis – after they had settled (Figure 1 shows axis orientations). These tests were undertaken on the uniaxial test device, with a 1 kN load cell, at a strain rate of 0.0133 s^{-1}, with a preload of 0.5 N and a sampling rate of 48 Hz. Compression tests were filmed using two synchronized cameras (Phantom Miro, R111 & Nikon, AF Nikkor 24 – 85 mm lens), recording at 24 fps with 85 mm optical zoom and a resolution of 1,280 × 800 p (**Figure 3**a). Speckle patterns (Figure 3b to c) were applied to the white foam using a small point black marker pen (Staedtler, Lumocolour), to facilitate full-field strain measurements by 3D digital image correlation (DIC). Samples were rotated between tests, so the horizontal camera field of view was parallel to the x, then z, then x-axis – facilitating ν_{zx}, ν_{xz} then ν_{yx} measurements.

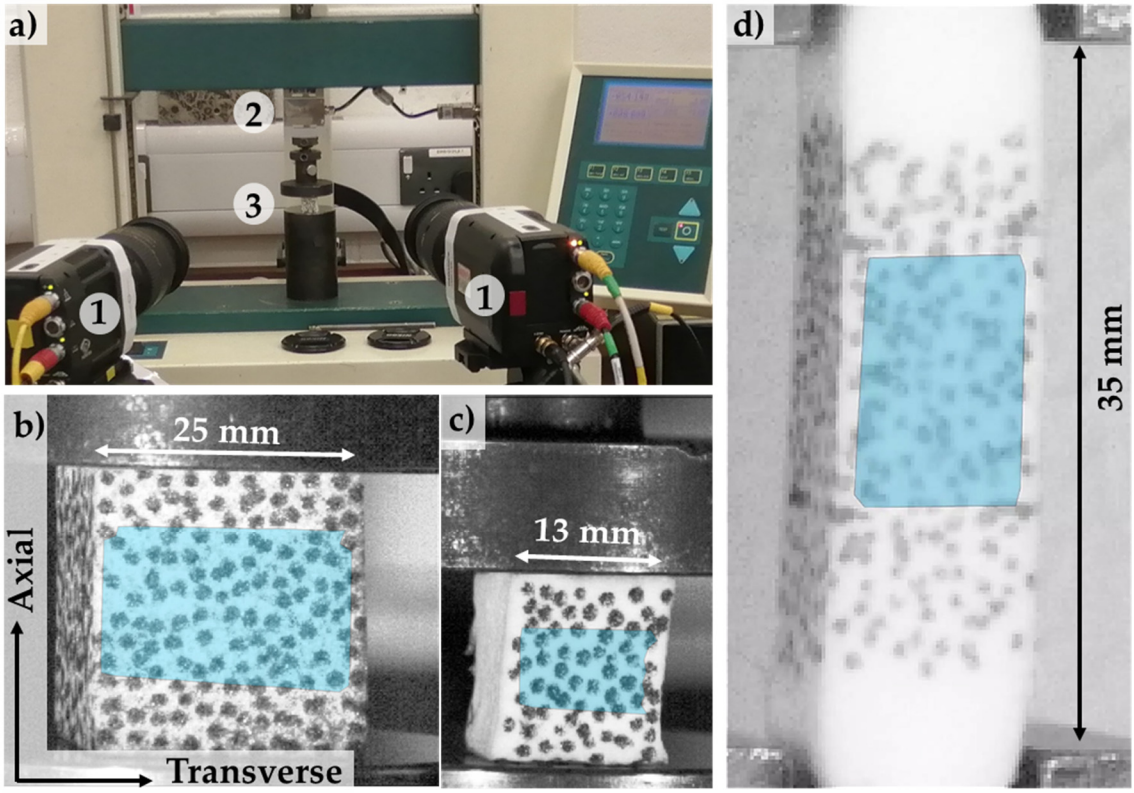

Figure 3: *Mechanical test set up showing a) cameras (1), load cell (2) and foam and compression plates (3) – with lights placed to the outside of the cameras (outside the image); b) to d) left hand camera image of b) compression test of an unconverted cube; c) compression test of a processed cube (FVR = 3.5); d) tensile test of a processed sample (FVR = 2.5) (all LD-45 before loading). Axes in (b) clarify naming conventions used throughout. Target area for DIC shaded blue in (b) to (d).*

Camera calibration was undertaken using a GOM CP20MV 72 × 90 mm calibration board, with video footage analysed in GOM Correlate Professional (2018). A target area was defined over the central third of each cube (Figure 3b to c), to mitigate frictional end effects, over which mean axial and transverse engineering strains were calculated, with matching against definition stage. While the cameras could not be synchronised with the uniaxial test device, data from each system was matched manually. The end of each test was identified as the point when the axial strain (DIC) or displacement (test device) became constant, and the start was

then located – 15 seconds before this. Polynomial trend lines were fitted to axial engineering strain vs. time data (Pearson's r^2 = 1.00 ± 0.00) and used to recalculate axial strain at time intervals recorded by the uniaxial test device. Young's moduli were calculated by fitting straight lines to stress vs. DIC strain data, over the initial linear stress vs. strain region (0 to 5.75 ± 3.00%, r^2 = 0.99 ± 0.02), with engineering stress calculated from device force and sample measurements taken before each test. Poisson's ratios were calculated by fitting straight lines to DIC transverse vs. axial engineering strain data, over the initial linear region (0 to 5.24 ± 2.64%, r^2 = 0.89 ± 0.19). All r^2 values indicate strong (0.70 to 0.89) or very strong (0.9 to 1.0) correlations [25].

Tensile tests (Figure 3d) were applied to ~8 × 8 × 50 mm cuboids cut from the centre of the processed large samples (original dimensions of 75 × 25 × 25 mm) – with textured device jaws clamping over a length of 7.5 mm to a thickness of ~1 mm. Each of the three cuboids was tested twice – both in the long y-axis, with the camera field of view parallel to first the x, then the z-axis – facilitating ν_{yx} then ν_{yz} measurements.

3. Results

3.1 Sample measurements

Settling lasted up to three months, before sample volumes varied by under 10% for three consecutive weeks. Settling time reduced to within 24 hours following post-processing in the vacuum chamber (Supplementary Figure S4). The measured density of the unconverted LD-45 foam was 39.74 ± 1.39 kg/m^3, while that of the LD-24 foam was 21.26 ± 0.63 kg/m^3, both slightly below expected values of 45 and 24 kg/m^3, respectively. There was negligible (<0.5%) mass loss after processing. FVRs were between two and five (**Figure 4**), covering the range that gave a negative Poisson's ratio with steam processing of similar foam [40]. FVR increased with both the processing pressure, and the number of processing cycles (Figure 4a) – although outliers with low FVRs were noticed at the highest pressure of 700 kPa. These outlying samples were processed towards the end of the study – when relative humidity was higher (52.4 ± 7.6) than at the beginning (40.3 ± 2.3%). For the same processing conditions, similar FVRs were achieved for samples of varying original size (Figure 4b). Unlike with steam processing methods [40,48], the original aspect ratio of the foam barely effected the amount of compression in each axis (Figure 4c). Indeed, linear compression ratios (LCR, final/original length) were similar for each foam (Supplementary Figure S5).

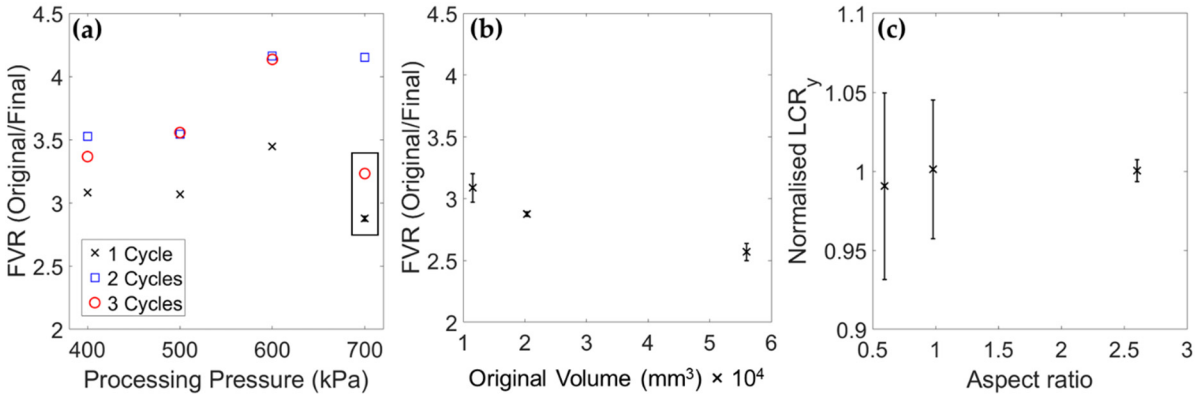

Figure 4: *Sample measurement data: a) Final volume ratio (FVR) vs. processing pressure, with outliers labelled; b) original sample volume vs. FVR, for LD-45 samples fabricated in one cycle at 700 kPa; c) aspect ratio (y dimensions / mean of x and z) vs. normalised* LCR_y *(*LCR_y *multiplied by the cube route of FVR).*

3.2 Cellular Structure

Microscopic images show the unconverted foam hexagonal cellular structure (**Figure 5**a & b), and the processed foam's kinked cell walls (Figure 5c to f), characteristic of an auxetic foam. The elongated cell rise present in some foams, and typically visible under microscopy [54], was not seen in either of the unconverted foams used here (Figure 5a & b; Supplementary Figure S6 shows LD-24 cellular structures). Similarly, differences between planes were not seen for the processed samples (i.e., between Figure 5c & d, or Figure 5e & f), but the higher FVR foam (FVR = 4, Figure 5e & f) had visibly smaller cells than when the FVR was three (Figure 5c & d). Trends for the two foams were similar, but the LD-24 had a less dense cellular structure than the LD-45 (Supplementary Figure S6), as expected.

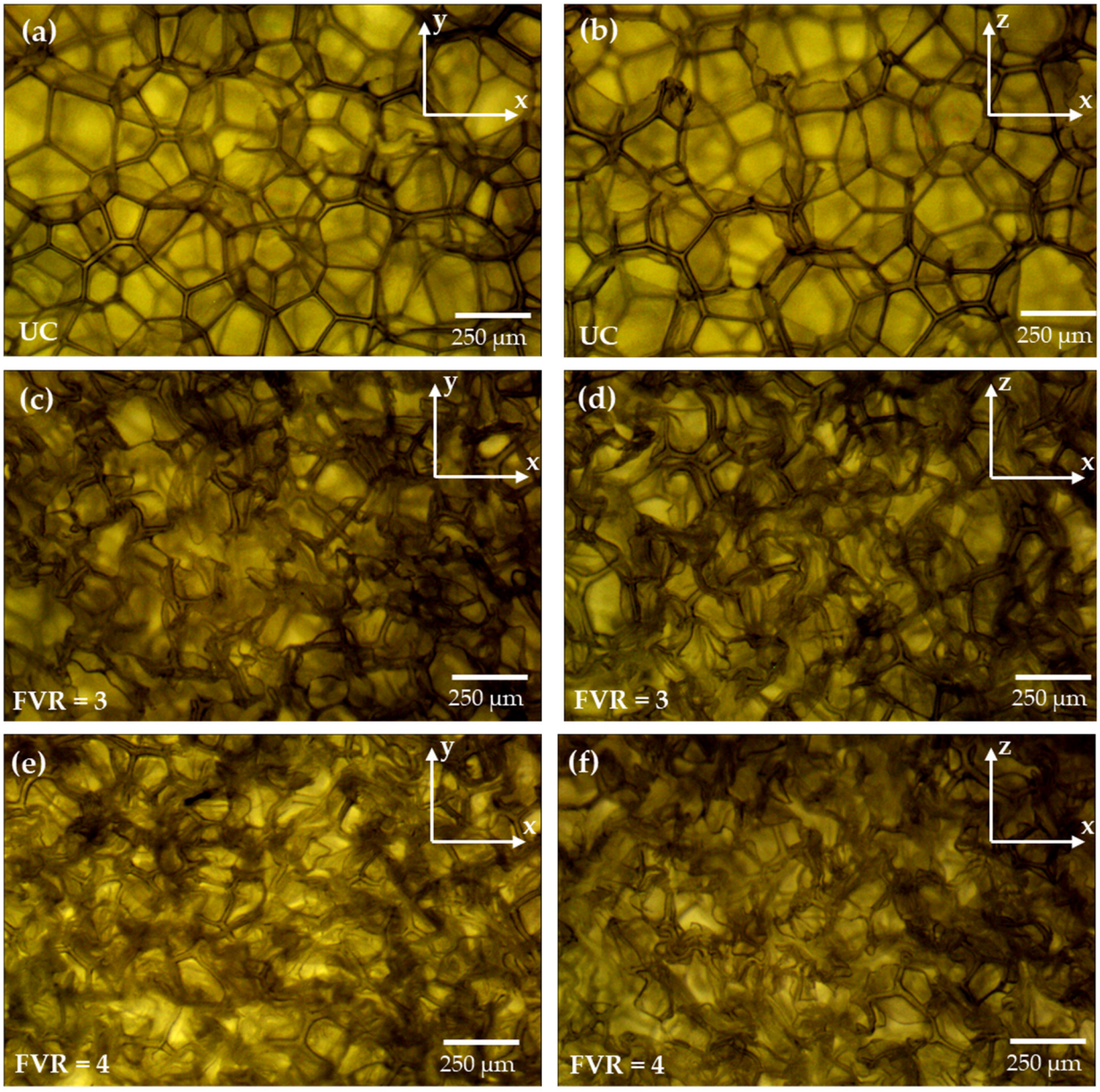

Figure 5: *Microscopic images of LD-45 taken at three times magnification, showing the cellular structure, when a) & b) unconverted, and with an FVR of c) & d) three, and e) & f) four. a), c) & e) show the y-x plane, while b), d) & f) show the z-x plane. Axes labelled in figures show the planes.*

3.3 Digital Image Correlation

DIC contour plots show positive transverse strain (and positive Poisson's ratio ν_{zx}) in compression for the unconverted foam, as expected, increasing in magnitude between 10 (2%, mostly green, **Figure 6**a) and 20% compression (3%, green and yellow, Figure 6b). Processed foam exhibited auxetic ν_{zx}, transverse contraction in compression, decreasing in magnitude between 10 (−1%, mostly dark blue, Figure 6c) and 20% compression (> −1%, mixture of light and dark blue, Figure 6d). Auxetic ν_{xy} transverse expansion was seen in tension, increasing in magnitude between 10 (1%, mostly light blue, Figure 6e) and 20% compression (>1%, mostly light blue with darker regions, Figure 6e). The supplementary video shows the tests in Figure 6. **Figure 7**a shows the same trends as **Figure 6**; transverse expansion in compression for the

unconverted cube, transverse contraction then expansion beyond ~10% compression for the processed cube, and transverse expansion in tension (Figure 7a).

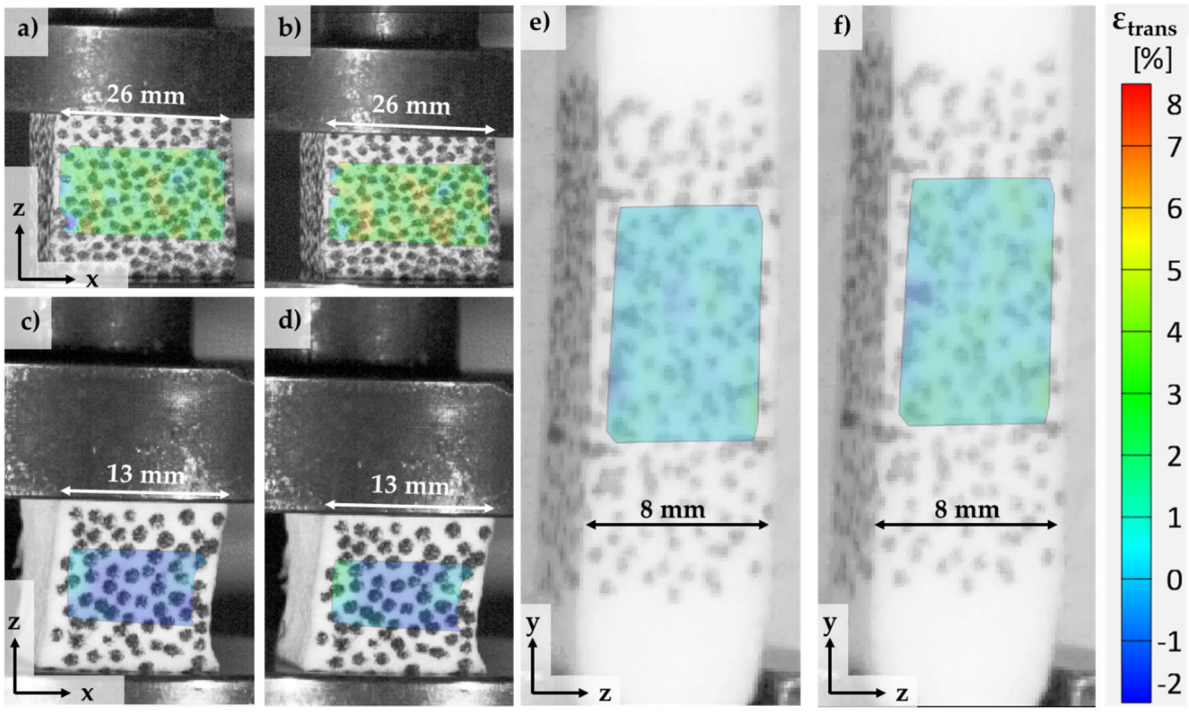

Figure 6: *DIC contour plots showing transverse strain of LD-45 foam; a) & b) unconverted at a) 10% and b) 20% compression; c) & d) processed (FVR = 3.5) at c) 10% and d) 20% compression; e) & f) processed (FVR = 2.5) at e) 10% and f) 20% tension. All contour plots are overlaid on the left camera image and use the same legend. Axes in a), c) & e) show sample orientation.*

3.4 Poisson's ratios

A mean Poisson's ratio was taken over the three axes, based on similarity in cellular structure and LCR between orientations, and similar trends in FVR vs. direction dependent Poisson's ratio data (Supplementary Figure S7). The Poisson's ratio vs. FVR data for these processed cubes agree with studies using open cell foam (e.g. [43,55–59]); reducing to negative values between FVRs of 1.0 and 2.5 (lowest Poisson's ratios here were about -0.2, Figure 7), then plateauing or marginally increasing towards zero at an FVR of five. The samples tested in tension were auxetic at a lower FVR (<2.5) than those tested in compression [43,55,56].

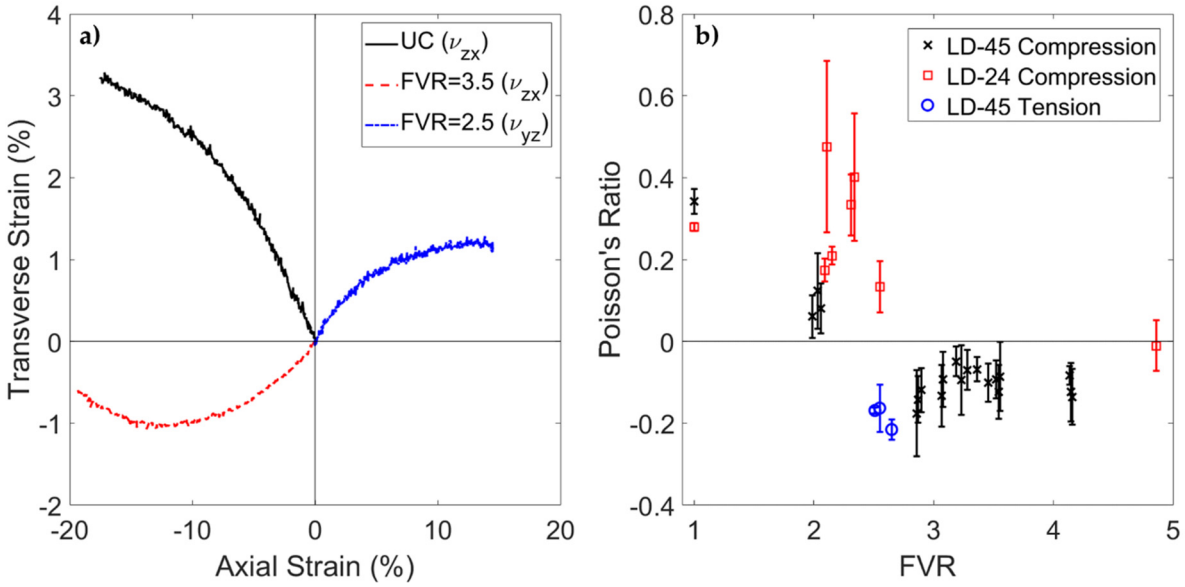

Figure 7: *a) Sample DIC transverse vs. axial strain plots, and b) mean Poisson's ratio (between orientations, calculated over the initial linear transverse vs axial strain region up to 5.24 ± 2.64%) vs. FVR data (FVR = 1 is the unconverted foam data). Error bars show one standard deviation.*

3.5 Young's moduli

The unconverted foam compressive strain data was non-linear, with a plateau region between 5 and 10% compression (**Figure 8**a) – as expected [40,48,54,60,61]. As with Poisson's ratio data, mean values for Young's moduli are presented – with direction dependent values in supplementary Figures S7 and S8. The LD-24 foam had lower Young's moduli than the LD-45 (Figure 8b), as expected due to its lower density, and therefore lower ratio of cell wall thickness to length [54,61]. Some samples showed high variation in Young's modulus between orientations (Figure 8b) – although this did not appear to be a consistent trend (Figure S8), so did not suggest anisotropy. Variation between orientations was more likely related to "wasting" of sample edges (visible in Figure 6c & d), which became concave under applied pressure, as expected [42], meaning samples were not always cubic. Lower variation in Young's modulus was noticed in the more uniform tensile samples. The trends between FVR and normalised Young's moduli, which were; an initial decrease in Young's modulus up to an FVR of ~3.5, then constant or increasing Young's moduli up to an FVR of five, agree with previous work on open cell foam [43,58,59]. Compressive Young's moduli, Poisson's ratio and FVR data are collated in supplementary Table S2 (LD-45) and S3 (LD-24).

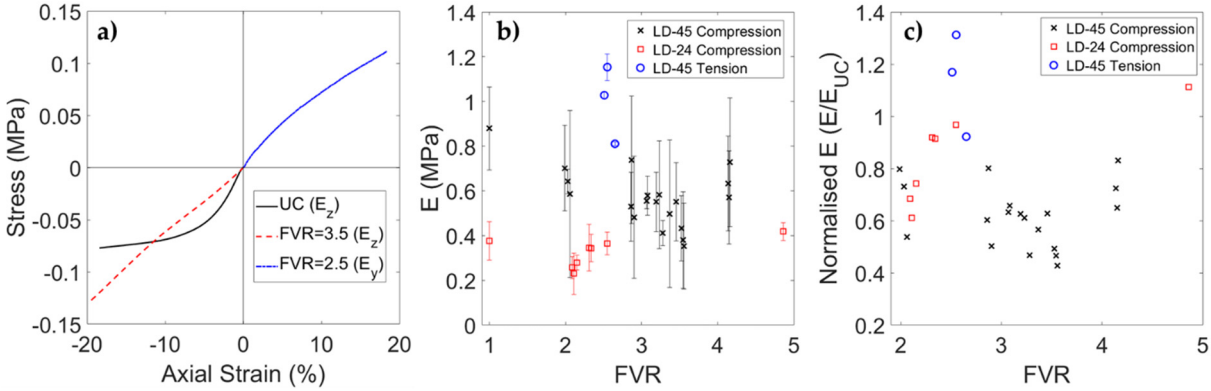

Figure 8: *a) Sample stress vs. axial strain plots, b) mean Young's moduli (between orientations, calculated over the initial linear transverse vs axial strain region up to 5.75 ± 3.00%) vs. FVR data (FVR = 1 is the unconverted foam data, error bars show one standard deviation) and c) Young's moduli, normalised to unconverted foam Young's modulus, vs. FVR.*

With the high standard deviations for Young's moduli in Figure 8b, a symmetric compliance matrix is included as a measure of data reliability [19] (Supplementary Figure S9). Pearson's r^2 between $E_x \times \nu_{zx}$ and $E_z \times \nu_{xz}$ was 0.94, suggesting a very strong correlation [25] and reliable data. Auxetic samples, with negative $E_x \times \nu_{zx}$ and $E_z \times \nu_{xz}$, and concave edges (most prevalent in their planar x and y axes, Figure 6c & d), deviated most from the symmetric compliance condition.

4. Discussion

We have clarified a method for making auxetic closed cell foam in a pressure vessel (Supplementary Materials Figure S1 & Table S1). Increasing the processing pressure caused the foam to shrink more (increased FVR), other than for some outlying cases collected towards the end of the study (Figure 4a). The outlying FVRs may have been caused by higher relative humidity recorded both when processing these samples and while they settled. Moisture can promote cross-linking in polyethylene [62], which may have fixed cellular structures sooner in these samples, causing them to shrink less than those stored at lower relative humidity. As such, further work should control relative humidity while processing such foams that are suspectable to moisture.

The results suggest that the pressure vessel method is less sensitive to original foam aspect ratio and volume than steam processing methods [40,48] – producing quasi-isotropic samples (Figures 4, 5, 7 & 8). Interestingly, trends between FVR, cellular structure and mechanical properties also agree with work on auxetic open cell foam (e.g. [43,55–59]). This finding indicates that the extensive structure-property knowledge base for auxetic open cell foam, dating back thirty years, can be broadly applied to auxetic closed cell foams. Broadly, higher FVR increases the number, and inward angle, of kinked cell ribs [1,43,63,64], as shown in Figure 5. As FVR increases, Poisson's ratio reduces – first towards zero, then to increasing magnitude negative values (Figure 7b), as explained by Gibson & Ashby's hinging, and combined rib bending and hinging, analytical models for hexagonal honeycombs [54].

The long settling time for the processed foam of up to three months may cause problems for commercial manufacture and uptake. Placing the processed foam in a vacuum reduced the fabrication and settling duration to within 24 hours – which is faster than the current steam

processing method (whereby samples must be dried after conversion [40]). The previous pressure vessel study used longer processing times (of ~24 hours), and found foam settled after about three weeks [42]. It is likely that there would be more options to further reduce processing and settling time, to save fabrication costs and energy, by adjusting processing conditions. As settling time can be reduced by placing the processed foam in a vacuum, such work will be simpler; removing the need to monitor foam for several weeks or months with a view to save hours during processing.

Efforts can now focus on using larger pressure vessels to make larger auxetic closed cell foam samples. Such larger samples could address limitations to this work, where ASTM D3574 – 11 compliant test samples could not be cut out and tested [53]. Larger samples would also facilitate prototyping and impact testing for sports applications [10,65,66], footwear [67] and other protective equipment. Indeed, scaled up, streamlined procedures, and optimised processing conditions, could help bring auxetic closed cell foam to the various potential commercial applications (e.g., sporting goods, medical devices, defence, aerospace and marine vessels). Combining pressure based and "one-pot" fabrication methods could be of particular interest [38,39] – with potential to make larger samples using any polymer (pressure method benefits) more quickly and efficiently ("one-pot" benefits).

Without relying on the boiling point of water, or other liquids, the pressure vessel method could potentially be applied to more closed cell foams, particularly those made from polymers that do not soften close to 100°C. Such polymers commonly used to make closed cell foam include polyurethane (which can soften above 180°C [1,44]) and some EVAs (which can melt at 65°C [45–47]). The wider range of potential foams opens new applications; with EVA's improved damping making it more suitable to impact protection [68,69] than the polyethylene foam used in most auxetic closed cell foam fabrications [39–41,48]. Future work could use this pressure vessel method with a broader range of foams made from different polymers, adjusting processing temperatures to match the foam softening temperatures.

With the increasing options to make auxetic closed cell foam, further work can focus on more detailed characterisation and application-based testing. For open cell auxetic foam, shear modulus [14,18], indentation resistance [70–72], impact performance [9,10,73,74], vibration damping [11,12,14], and energy absorption [8,10,16] have all been studied. Auxetic closed cell foam studies have only focussed on fabrication [39–41,48], and high strain rate testing [60]. With conventional closed cell foam being common for impact protection and energy absorption [20,21,24]devices, indentation and impact studies – targeting potential benefits of auxetic behaviour [1,7,8] – could be focusses of further work.

5. Conclusions

Increasing the processing pressure, and number of cycles (i.e., cumulative processing duration), increased the final volume ratio of closed cell foam made in a pressure vessel within an oven. Unlike with steam processing, final volume ratio barely reduced with increasing original foam volume (same processing conditions) and changing the aspect ratio did not cause anisotropy. Further, this method – unconstrained by the boiling point of water – has the potential to be applied to more foam types than steam processing. As with open cell foam,

final volume ratios of two to five provided auxetic foams – with the lowest negative Poisson's ratios (of about -0.2) at a final volume ratio of three. Young's moduli reduced between final volume ratios of 1.0 and 2.5, then remained constant or marginally increased. A settling time of up to three months under ambient conditions, where samples slowly shrank after processing, was reduced to within 24-hours by post-processing in a vacuum.

Acknowledgements

This work was funded by ON AG (Zurich, Switzerland) and Manchester Metropolitan University. The authors declare no conflicts of interest. We would like to thank technicians at Manchester Metropolitan University for their assistance with fabrication and testing – particularly Michael Green, John Penfold and Stephen Lloyd.

References

1. Jiang W, Ren X, Wang SL, Zhang XG, Zhang XY, Luo C, et al. Manufacturing, characteristics and applications of auxetic foams: A state-of-the-art review. Compos Part B Eng. 2022.235. 109733.
2. Shepherd T, Allen T, Winwood K, Venkatraman PD, Alderson A. Validation of a Finite Element Modelling Process for Auxetic Structures under Impact. Phys Status Solidi B Basic Solid State Phys. 2020.1900197.
3. Hanna B, Adams R, Townsend S, Robinson M, Soe S, Stewart M, et al. Auxetic Metamaterial Optimisation for Head Impact Mitigation in American Football. Int J Impact Eng. 2021. 103991.
4. Chung VWJ, Dias L, Booth G, Cripton PA. Clinical Biomechanics Incorporating neck biomechanics in helmet testing : Evaluation of commercially available WaveCel helmets. Clin Biomech. 2022.94(August 2021). 105628.
5. Dudek KK, Iglesias Martınez JA, Ulliac G, Kadic M. Micro-scale Auxetic Hierarchical Mechanical Metamaterials for Shape Morphing. Adv Mater. 2022.
6. Valente J, Plum E, Youngs IJ, Zheludev NI. Nano- and Micro-Auxetic Plasmonic Materials. Adv Mater. 2016.28(26). 5176–80.
7. Evans KE, Alderson A. Auxetic materials: Functional materials and structures from lateral thinking! Adv Mater. 2000.12(9). 617–28.
8. Duncan O, Shepherd T, Moroney C, Foster L, Venkatraman PD, Winwood K, et al. Review of auxetic materials for sports applications: Expanding options in comfort and protection. Appl Sci. 2018.8(6). 941.
9. Zhang Q, Scarpa F, Barton D, Zhu Y, Lang Z, Zhang D, et al. Impact properties of uniaxially thermoformed auxetic foams. Int J Impact Eng. 2022. 104176.
10. Duncan O, Foster L, Senior T, Alderson A, Allen T. Quasi-static characterisation and impact testing of auxetic foam for sports safety applications. Smart Mater Struct. 2016.25(5). 054014.
11. Bianchi M, Scarpa F. Vibration transmissibility and damping behaviour for auxetic and conventional foams under linear and nonlinear regimes. Smart Mater Struct. 2013.22(8).
12. Scarpa F, Giacomin J, Zhang Y, Pastorino P. Mechanical performance of auxetic polyurethane foam for antivibration glove applications. Cell Polym. 2005.24(5). 253–68.
13. Scarpa F, Ciffo LG, Yates JR. Dynamic properties of high structural integrity auxetic open cell foam. Smart Mater Struct. 2003.13(1). 49–56.
14. Chun Checn H, Scarpa F, Hallak Panzera T, Farrow I, Peng H-X. Shear stiffness and energy absorption of auxetic open cell foams as sandwich cores. Phys Status Solidi. 2018.256(1). 1–9.
15. Moroney C, Alderson A, Allen T, Sanami M, Venkatraman P. The Application of Auxetic Material for Protective Sports Apparel. Proceedings. 2018.2(6). 251.
16. Sanami M, Ravirala N, Alderson K, Alderson A. Auxetic materials for sports applications. Procedia Eng. 2014.72. 453–8.
17. Scarpa F. Auxetics in smart systems and structures 2015. 2016. 1.
18. Novak N, Duncan O, Allen T, Alderson A, Vesenjak M, Ren Z. Shear modulus of conventional and auxetic open-cell foam. Mech Mater. 2021. 104743.
19. Timoshenko SP, Goodier JN. Theory of Elasticity. 3rd ed. New York: McGraw-Hill, USA; **1970**.
20. Ankrah S, Mills NJ. Performance of football shin guards for direct stud impacts. Sport Eng. 2003.6(4). 207–19.

21. Ankrah S, Mills NJ. Analysis of ankle protection in Association football. Sport Eng. 2004.7(1). 41–52.
22. Calvert KL, Trumble KP, Webster TJ, Kirkpatrick LA. Characterization of commercial rigid polyurethane foams used as bone analogs for implant testing. J Mater Sci Mater Med. 2010.21(5). 1453–61.
23. Sanders JE, Greve JM, Mitchell SB, Zachariah SG. Material properties of commonly-used interface materials and their static coefficients of friction with skin and socks. J Rehabil Res Dev. 1998.35(2). 161–76.
24. Gokhale AA, Ravi Kumar N V., Sudhakar B, Sahu SN, Basumatary H, Dhara S. Cellular metals and ceramics for defence applications. Def Sci J. 2011.61(6). 567–75.
25. Schober P, Schwarte LA. Correlation coefficients: Appropriate use and interpretation. Anesth Analg. 2018.126(5). 1763–8.
26. Luong DD, Pinisetty D, Gupta N. Compressive properties of closed-cell polyvinyl chloride foams at low and high strain rates: Experimental investigation and critical review of state of the art. Compos Part B Eng. 2013.44(1). 403–16.
27. Lakes RS. Foam Structures with a Negative Poisson's Ratio. Science (80-). 1987.235(4792). 1038–40.
28. Zhang Q, Lu W, Scarpa F, Barton D, Lakes RS, Zhu Y, et al. Large stiffness thermoformed open cell foams with auxeticity. Appl Mater Today. 2020.20. 100775.
29. Li Y, Zeng C. Room-Temperature, Near-Instantaneous Fabrication of Auxetic Materials with Constant Poisson's Ratio over Large Deformation. Adv Mater. 2016.28(14). 2822–6.
30. Bianchi M, Scarpa F, Banse M, Smith CW. Novel generation of auxetic open cell foams for curved and arbitrary shapes. Acta Mater. 2011.59(2). 686–91.
31. Grima JN, Attard D, Gatt R. A novel process for the manufacture of auxetic foams and for the conversion of auxetic foam to conventional form (WO 2010049511 A2). 2010. 1–5.
32. Zeng C, Li Y. Material systems and methods of manufacture for auxetic foams (WO2016014782A1). 2016. p. 1–17.
33. Bianchi M, Scarpa F. Method of manufacturing a foam. Vol. 2. US Patents; 8,313,682 B2, 2012. p. 1–5.
34. Alderson A, Alderson KL, Davies PJ, Smart GM. Process for the preparation of auxetic foams. Vol. 2. US Patents; US 8,277,719 B2, 2012. p. 1 to 4.
35. Hu H, Lai Z, Ding G, Zhuang D. Experimental investigation on water drainage characteristics of open-cell metal foams with different wettabilities. Int J Refrig. 2017.79. 101–13.
36. Mills NJ. Chapter 20 - The effects of water. In: Mills NJ, editor. Polymer Foams Handbook. Oxford, UK: Butterworth-Heinemann; **2007**. p. 479–501.
37. Mills NJ. Chapter 8 - Air flow in open-cell foams. In: Mills NJ, editor. Polymer Foams Handbook. Oxford, UK: Butterworth-Heinemann; **2007**. p. 117–203.
38. Li N, Liu Z, Shi X, Fan D, Xing H, Qiu J, et al. Preparing Polypropylene Auxetic Foam by a One-pot CO 2 Foaming Process. Adv Eng Mater. 2021.2100859. 1–10.
39. Fan D, Shi Z, Li N, Qiu J, Xing H, Jiang Z, et al. Novel Method for Preparing a High-Performance Auxetic Foam Directly from Polymer Resin by a One-Pot CO2 Foaming Process. ACS Appl Mater Interfaces. 2020.12. 48040–8.
40. Duncan O, Allen T, Birch A, Foster L, Hart J, Alderson A. Effect of steam conversion on the cellular structure, Young's modulus and negative Poisson's ratio of closed cell foam. Smart Mater Struct. 2020.30. 015031.
41. Fan D, Li M, Qiu J, Xing H, Jiang Z, Tang T. Novel Method for Preparing Auxetic Foam from Closed-Cell Polymer Foam Based on the Steam Penetration and Condensation Process. ACS Appl Mater Interfaces. 2018.10(26). 22669–22677.
42. Martz EO, Lee T, Lakes RS, Goel VK, Park JB. Re-entrant transformation methods in closed cell foams. Cell Polym. 1996.15(4). 229–49.
43. Duncan O, Clegg F, Essa A, Bell AMT, Foster L, Allen T, et al. Effects of Heat Exposure and Volumetric Compression on Poisson's Ratios, Young's Moduli, and Polymeric Composition During Thermo-Mechanical Conversion of Auxetic Open Cell Polyurethane Foam. Phys Status Solidi. 2019.256(1800393). 1–12.
44. Critchley R, Corni I, Wharton JA, Walsh FC, Wood RJK, Stokes KR. A review of the manufacture, mechanical properties and potential applications of auxetic foams. Phys Status Solidi Basic Res. 2013.250(10). 1963–82.
45. Blieske U, Stollwerck G. Glass and other encapsulation materials. 1st ed. Vol. 89, Semiconductors and Semimetals. Elsevier Inc.; **2013**. 199–258 p.
46. Henderson AM. Ethylene-vinyl acetate (EVA) copolymers: a general review. 1993.(1).
47. Thorne JL, Crawford RJ. 2 - ROTATIONAL MOLDING POLYMERS. In: In Plastics Design Library,

Rotational Molding Technology. Science Direct; **2002**. p. 19–68.
48. Duncan O, Alderson A, Allen T. Fabrication, characterisation and analytical modelling of gradient auxetic closed cell foams. Smart Mater Struct. 2021.30(035014).
49. Tong JWK, Ng EYK. Preliminary investigation on the reduction of plantar loading pressure with different insole materials (SRP – Slow Recovery Poron®, P – Poron®, PPF – Poron® + Plastazote, firm and PPS – Poron® + Plastazote, soft). Foot. 2010.20. 1–6.
50. Kermen E, Mohammadi H. Mechanics of foot orthotics: material properties. J Med Eng Technol. 2021.45(8). 627–41.
51. Meng Y, Yang L, Jiang X, István B, Gu Y. The Effectiveness of Personalized Custom Insoles on Foot Loading Redistribution during Walking and Running. J Biomimetics, Biomater Biomed Eng. 2020.44. 1–8.
52. Sanders JE, Daly CH. How does vacuum forming affect Pelite mechanical properties? Prosthet Orthot Int. 1994.18(1). 43–8.
53. Annual Book of ASTM Standards. Standard Test Methods for Flexible Cellular Materials — Slab, Bonded, and Molded Urethane Foams. Annual Book of ASTM Standards 2008.
54. Gibson LJ, Ashby MF. Cellular solids. Structure and properties. Cambridge: Press Syndicate of the University of Cambridge; **1997**. 67, 176–183, 259–264, 286, 301, 498 p.
55. Critchley R, Smy V, Corni I, Wharton JA, Walsh FC, Robert JK, et al. Experimental and computation assessment of thermomechanical effects during auxetic foam fabrication. Sci Rep. 2020.10(18301).
56. Duncan O, Allen T, Foster L, Gatt R, Grima JN, Alderson A. Controlling Density and Modulus in Auxetic Foam Fabrications—Implications for Impact and Indentation Testing. Proceedings. 2018.2(6). 250.
57. Choi JB, Lakes RS. Non-linear properties of polymer cellular materials with a negative Poisson's ratio. J Mater Sci. 1992.27(17). 4678–84.
58. Bianchi M, Scarpa F, Smith CW. Shape memory behaviour in auxetic foams: Mechanical properties. Acta Mater. 2010.58(3). 858–65.
59. Boba K, Bianchi M, McCombe G, Gatt R, Griffin AC, Richardson RM, et al. Blocked shape memory effect in negative Poisson's ratio polymer metamaterials. ACS Appl Mater Interfaces. 2016. acsami.6b02809.
60. Duncan O, Bailly N, Allen T, Petit Y, Wagnac E, Alderson A. Effect of compressive strain rate on the Poisson's ratio of auxetic foam. Appl Sci. 2021.11(3).
61. Mills NJ, Zhu HX. The high strain compression of closed-cell polymer foams. J Mech Phys Solids. 1999.47(3). 669–95.
62. Pape PG. Moisture crosslinking process for foamed polymers. J Vinyl Addit Technol. 2000.6(1). 49–52.
63. Zhang Q, Lu W, Scarpa F, Barton D, Rankin K. Topological characteristics and mechanical properties of uniaxially thermoformed auxetic foam. Mater Des. 2021.211.
64. Chan N, Evans KE. Microscopic examination of the microstructure and deformation of conventional and auxetic foams. J Mater Sci. 1997.2. 5725–36.
65. Allen T, Shepherd J, Hewage TAM, Senior T, Foster L, Alderson A. Low-kinetic energy impact response of auxetic and conventional open-cell polyurethane foams. Phys Status Solidi Basic Res. 2015.9. 1–9.
66. Foster L, Peketi P, Allen T, Senior T, Duncan O, Alderson A. Application of Auxetic Foam in Sports Helmets. Appl Sci. 2018.8(3). 354.
67. Duncan O, Naylor G, M JG, Allen T, Foster L, Hart J, et al. Plantar Pressure Distribution under Uniform and Gradient Foam during Running and Jumping †. Proc 13th Conf Int Sport Eng Assoc. 2020.49(116). 1–6.
68. Mills NJ, Fitzgerald C, Gilchrist A, Verdejo R. Polymer foams for personal protection: Cushions, shoes and helmets. Compos Sci Technol. 2003.63(16). 2389–400.
69. Even-tzur N, Weisz E, Hirsch-falk Y, Gefen A. Role of EVA viscoelastic properties in the protective performance of a sport shoe: Computational studies. Biomed Mater Eng. 2017.16(5). 289–99.
70. Chan N, Evans KE. Indentation resilience of conventional and auxetic foams. J Cell Plast. 1998.34. 231–60.
71. Lakes RS, Elms K. Indentability of conventional and negative Poisson's ratio foams. J Compos Mater. 1993.27(12). 1193–202.
72. Allen T, Duncan O, Foster L, Senior T, Zampieri D, Edeh V, et al. Auxetic foam for snow-sport safety devices. Snow Sport Trauma Saf Proc Int Soc Ski Saf. 2016.21.
73. Lisiecki J, Błazejewicz T, Kłysz S, Gmurczyk G, Reymer P, Mikułowski G. Tests of polyurethane foams with negative Poisson's ratio. Phys Status Solidi Basic Res. 2013.250(10). 1988–95.
74. Ge C. A comparative study between felted and triaxial compressed polymer foams on cushion performance. J Cell Plast. 2013.49(6). 521–33.